Journal of Nuclear Materials 390–391 (2009) 781–784

Contents lists available at ScienceDirect

Journal of Nuclear Materials

journal homepage: www.elsevier.com/locate/jnucmat

ELM filament interaction with the JET main chamber ☆

M.W. Jakubowski [a,b,*], W. Fundamenski [c], G. Arnoux [c], Th. Eich [a], R.A. Pitts [d], D. Reiter [b], R.C. Wolf [a], JET-EFDA contributors [e]

[a] Max-Planck-Institut für Plasmaphysik, EURATOM-IPP Association, Garching and Greifswald, Germany
[b] Forschungszentrum Jülich, Institut für Energieforschung (Plasmaphysik), EURATOM-FZJ Association, Trilateral Euergio Cluster, Jülich, Germany
[c] EURATOM-UKAEA Association, Culham Science Centre, OX14 3DB Abingdon, UK
[d] École Polytechnique Fédérale de Lausanne (EPFL), Centre de Recherches en Physique des Plasmas, Association EURATOM-Confédération Suisse, 1015 Lausanne, Switzerland
[e] JET-EFDA, Culham Science Centre, OX14 3DB Abingdon, UK

ARTICLE INFO

PACS:
52.55.Fa
52.55.Rk
52.40.Hf

ABSTRACT

This work constitutes the first extended analysis of the spatial structure of Type-I ELM filament footprints on the JET outer limiters and upper dump plates. The data is obtained using a wide angle infrared diagnostic (with time resolution of 125 Hz) and concerns ELMs with energy in the range $0.07 \leqslant \Delta W_{\mathrm{ELM}}/W_{\mathrm{ped}} \leqslant 0.32$. Type-III ELM filaments are not observed to deposit significant heat loads. The typical poloidal width of an ELM filament footprint is of order of 4–10° on the outer limiters and of order of 1–4° on the upper dump plates with weak linear dependence on the ELM size. Their quasi-toroidal mode numbers are in the range of 30–60 and 20–30, respectively.

1. Introduction

Edge localized modes (ELMs) are quasi-periodic MHD instabilities occurring as a result of pedestal pressure gradients found at the edge of H-mode plasmas [1]. In recent years, clear evidence of the ELM as a filamentary structure [2] propagating radially ($v_r \approx 10^3$ m/s) across the scrape-off layer (SOL) and extending far outside the separatrix [3,4] have been shown. This filamentary nature is also consistent with the non-linear ballooning mode theory [5], i.e. the peeling-ballooning mode, which is thought to be responsible for the evolution of the instability into several filamentary structures. The filaments are highly elongated along the magnetic field lines. By substracting two images (pre-ELM from post-ELM) obtained with the slow, visible camera at JET Ghendrih et al. in [6] were the first to find evidence for interaction between ELM filaments and the JET main chamber. This has been confirmed using infrared (IR) imaging on both JET [7,8] and ASDEX Upgrade [9–11]. A detailed discussion of radially propagating ELM filaments and the evolution of parallel losses may be found in a recent review paper [12].

ELMs can release up to 10% of the stored energy in a short amount of time (0.1–1 ms) and are therefore a serious threat for the safety of plasma-facing components (PFCs) in ITER, particulary the divertor target plates. Understanding ELM physics, topology and dynamics is essential if reliable extrapolations are to be made to ITER. Specifically, the heat fluxes deposited on the limiter tiles by the ELM filaments (up to ~ 10% of the total expelled energy [14]) have been less studied than divertor fluxes, but are a potential threat given the planned use of Be plasma-facing components on the ITER main chamber. It has been found on ASDEX Upgrade [9] that about 25% of the ELM energy is deposited on the first wall with a rather homogenous temperature pattern, when averaged over many ELM events [13]. In this contribution we present the first analysis of ELM filament footprints, for a wide range of ELM energies, on the outer limiters and upper dump plates of the JET main chamber. Recent results on visible imaging of filamentary nature of Type-I and Type-III ELMs on JET is discussed in [15].

2. Experimental set-up

Analysis of the spatial distribution of power deposition due to ELM filaments striking the main chamber PFCs have been performed with a wide angle infrared system. For the data presented here, the device was operated at a frame rate of 125 Hz and integration time of 60 μs. Low frame rate resolution does not allow to study the dynamics of the heat loads due to ELMs. The image is 512 × 408 pixels allowing simultaneous viewing of the outboard limiters and the upper dump plates with the resolution of a few millimeters. Fig. 1(a) shows the full frame view of the machine in infrared, as seen by the camera. The areas of interest to the analysis described in this paper are contained within the dashed lines. For

☆ See the Appendix of M.L. Watkins et al., Fusion Energy 2006 (Proceedings of the 21st International Conference Chengdu, 2006) IAEA.

* Corresponding author. Forschungszentrum Jülich, Institut für Energieforschung (Plasmaphysik), 52428, Jülich, Germany.
E-mail address: ma.jakubowski@fz-juelich.de (M.W. Jakubowski).

0022-3115/$ - see front matter © 2009 Elsevier B.V. All rights reserved.
doi:10.1016/j.jnucmat.2009.01.207

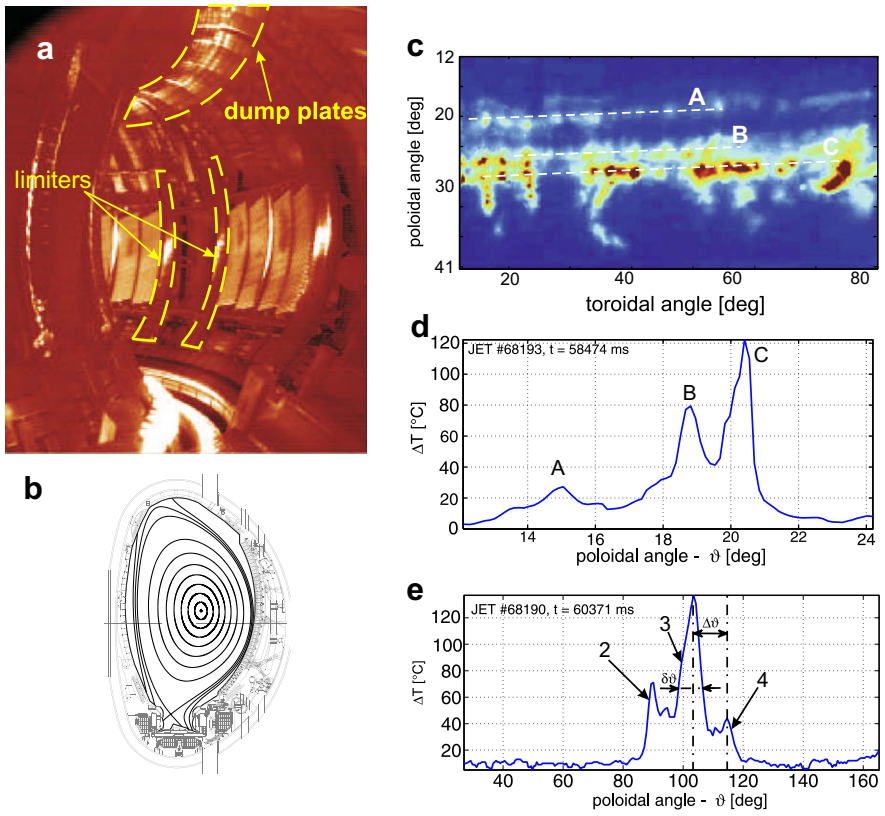

Fig. 1. (a) Wide angle view of the JET vessel with highlighted areas, where the analysis of the ELM power deposition zone is made. (b) EFIT reconstruction of the magnetic equilibrium for discharge #68190. (c) Image of the upper dump plate transformed to toroidal/poloidal plane. Three traces of the helically aligned filament footprint are visible (they are indicated with white dashed lines and labeled A, B and C). Example of the profile of Type-I ELM filament across upper dump plate (d) and along the left outer limiter (e). Values of poloidal angle (ϑ) in (e) increase towards the bottom of the vessel. Definition of $\delta\vartheta$ and $\Delta\vartheta$ is indicated in (e).

the analysis described below, the real space coordinates of these regions are mapped to toroidal and poloidal coordinates, helping to quantify the size and separation of the filament footprints.

Many of the results presented here are derived from measurements made in a short discharge series (#68190–#68196), all of which are characterized by a magnetic equilibrium with an ITER-like shape (see Fig. 1(c)). They have been operated at relatively high injected power (8–16 MW), plasma currents of 2.5 MA and 1.5 MA and toroidal fields of 2.5 T and 1.5 T respectively ($q_{95} = 3.3$). For this configuration the separatrix is in proximity of the upper dump plates (1–1.5 cm, when mapped to outer midplane), which makes them the first limiting surface. Even at these small distances, Type-III ELM filaments ($\Delta W \lesssim 50 - 60$ kJ for the investigated discharges) are not observed to deposit heat on the dump plates, nor on the outer limiters. In contrast, Type-I ELM filament footprints are observed over a wide range of ELM energies – 0.1 MJ $\leqslant \Delta W_{\mathrm{ELM}} \leqslant$ 0.8 MJ. ELMs smaller than 0.1 MJ do not create detectable power deposition imprints on the PFCs of the main chamber.

3. Structure of ELM filament footprints on main chamber PFCs

An example of an ELM filament footprint on the upper dump plate is shown in Fig. 1(c). This image is a difference of two IR frames (pre- and post-ELM), which were mapped onto the toroidal/poloidal plane. Clearly one recognizes areas of excess heat flux deposition, which are helically aligned. Three elongated structures have inclination angle of $\Delta\theta/\Delta\varphi \approx 0.07$, which is in very good agreement with pitch of magnetic field lines reconstructed with EFIT ($\Delta\vartheta/\Delta\varphi = 0.069$) for the time before the ELM crash. This agreement is consistently found for all cases of ELM filament dump plate interaction which have been studied. Typically there are two to four traces of ELM filaments, which appear at different poloidal angles with no preferential deposition location. It also seems that the number of structures is independent of the ELM size, in contrast to the footprints width ($\delta\vartheta$) and their separation ($\Delta\vartheta$). In order to quantify those values profiles along the poloidal coordinate are created. An example of the profile constructed from the area marked with dashed rectangle is presented in Fig. 1(e). As expected from the image in Fig. 1(c) there are three peaks visible at $\vartheta \approx 15^\circ, 19^\circ$ and 21°. For more detailed discussion of these quantities see Section 4.

The structure of the filament footprints on the surface of the outer limiters is analyzed in a similar way. An example of a typical poloidal profile of the surface temperature change due to filaments striking the limiter surface in these high triangularity discharges is presented in Fig. 1(d). There are three hot spots appearing located near the equatorial plane ($\vartheta = 90^\circ$), marked with labels 2, 3 and 4 in Fig. 1(e). There are also cases in which an additional one or two impact points are observed at higher or lower ϑ. In the majority of cases, interactions on the limiter surface occur preferentially near the equatorial plane (e.g. the peak labeled 3 in Fig. 1(e)) and have the highest amplitude there. This can be also seen in Fig. 2, where the histogram of the deposition location on the outer limiters is presented. The most preferred location for the power deposition falls into a range of ($100^\circ < \vartheta < 105^\circ$), to which there is shortest distance from the separatrix. Almost all traces of the filaments striking the surface of the limiter are located within the range of ($85^\circ < \vartheta < 115^\circ$). This is consistent with the results of experiments at DIII-D [16].

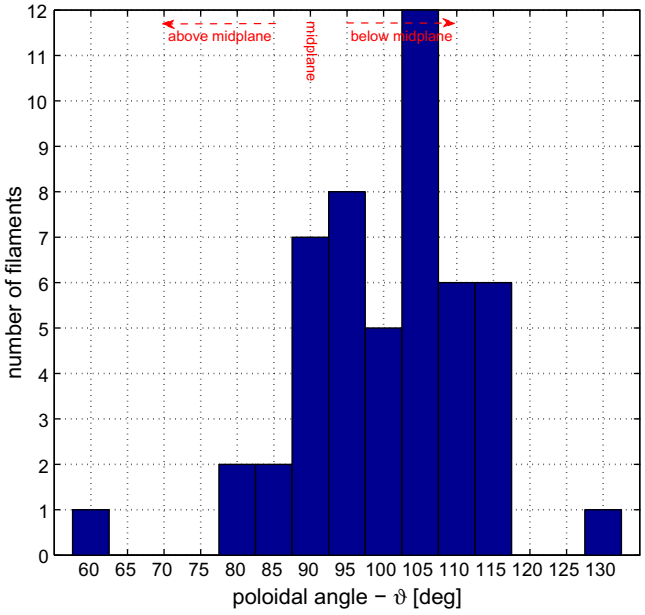

Fig. 2. Histogram of the position on the outer limiter, where the Type-I ELMs strike the surface.

To see more clearly the helical nature of ELM filament interactions on the outboard PFC's, Fig. 3(a) shows a full frame snapshot (inter-ELM background substracted) from the low triangularity discharge #66515, where there is little or no interaction with the upper dump plates and in which the first limiting flux surface resides near the outboard midplane. The shape of the equilibrium is presented in Fig. 3(b). A series of 3, poloidally separated hot spots are visible (highlighted by △, □ and ○), forming helically aligned structures. In order to compare them with the pre-ELM magnetic equilibrium they are mapped onto the poloidal/toroidal grid in Fig. 3(c) overlaid on which are the trajectories of field lines residing on a magnetic flux surface 6 cm from the separatrix at the outboard midplane (corresponding approximately to the radial location of the limiters). Here again filaments are well aligned with the pre-ELM calculated topology of the magnetic field lines. From the toroidal separation of three filaments $\Delta\varphi \approx 30^\circ$ implies quasi-toroidal mode number $n_{\mathrm{tor}} \approx 12$, what is roughly consistent with the peeling-ballooning model of ELM dynamics. A similar result was obtained in [6]. Both results, from upper dump plates and outer limiter suggest that the Type-I ELMs do not noticeably disturb the poloidal and toroidal components of the pre-ELM magnetic structure in the scrape-off layer.

4. Variation of footprint structure with ELM size

In the analysis here, ELM size (ΔW_{ELM} – obtained from fast diamagnetic loop measurements) is normalized to the pedestal stored energy, W_{ped}. The latter ($W_{\mathrm{ped}} = 3/2 \cdot n_e \cdot (T_e + T_i) \cdot V_{\mathrm{plasma}}$) is estimated using Thomson scattering measurements (n_e and T_e) and charge exchange recombination spectroscopy (T_i). Values of the pedestal stored energy are in the range 1.7–2 MJ, which is 30% of the plasma energy (W_{plasma} 5–6 MJ). The analysis have been performed over a wide range of ELM energies ($0.07 \leqslant \Delta W_{\mathrm{ELM}}/W_{\mathrm{ped}} \leqslant 0.32$). Results, expressed in terms of filament width ($\delta\vartheta$), quasi-toroidal mode number (n_{tor}) and ratio of filament width to separation ($\delta\vartheta/\Delta\vartheta$), are presented in Fig. 4(a) for the outer limiters and in Fig. 4(b) for the upper dump plates. Release of ELM energy to the PFCs of the main chamber is not axisymmetric but localized in the outer midplane as a set of helical events. Their separation is therefore described with the quasi-toroidal mode number, which can be calculated from the toroidal separation of filament footprints ($n_{\mathrm{tor}} = 2\pi/\Delta\varphi$). To obtain a value of $\Delta\varphi$ the relation between poloidal (n_{pol}) and toroidal mode number (n_{tor}) is used - $n_{\mathrm{tor}}/n_{\mathrm{pol}} = \Delta\vartheta/\Delta\varphi = \alpha$. In order to properly calculate the separation of the footprints on the outer limiters analysis has been performed for imprints near the equatorial plane. It is most likely that those structures result from adjacent filaments. They have been labeled 2, 3 and 4 in Section 3 and this nomenclature is maintained in Fig 4.

On the outer limiters filament widths show large scatter with no clear dependence on the ELM size. Widths vary between 4° (6 cm) and 8° (12 cm) with peak number 3 (see Fig. 1) being the widest for most of investigated ELM events. For the quasi-toroidal mode number most of the points cluster between $n_{tor} = 30$ and 40, corresponding to a footprint spatial separation of the order of 8–9°. This value seems to be constant for almost all investigated ELMs. Taking into account that both $\delta\vartheta$ and $\Delta\vartheta$ are constant with the ELM size, their ratio of them oscillates around a value of $\delta\vartheta/\Delta\vartheta = 0.8 \pm 0.2$.

In contrast to the outer limiters, both the filament footprint width and the filament separation have some dependence on ELM size, although, as before, the data are scattered. There is a trend for a linear increase of $\delta\vartheta$ with increasing ELM size from 1–2° (5 cm) at $\Delta W/W_{\mathrm{ped}} \approx 0.1$ to about 3° (11 cm) at

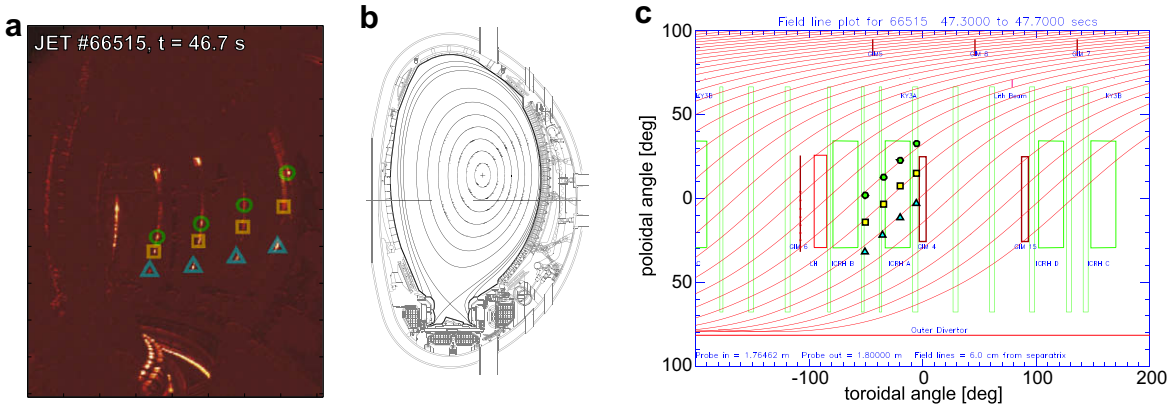

Fig. 3. (a) Wide angle infrared image illustrating footprints of Type-I ELM filaments deposited on the surface of the outer limiters during the discharge #66515. Footprints of three filaments are identified and marked with green, yellow and blue circles. (b) Reconstruction of the magnetic equilibrium for the discharge #66515. (c) The same footprints as in (a) mapped onto the vessel technical drawing and compared to the overlaid topology of the magnetic field lines from EFIT. Reconstruction is made for the magnetic flux surface deep in the scrape-off layer ($r - r_{\mathrm{sep}} = 6$ cm).

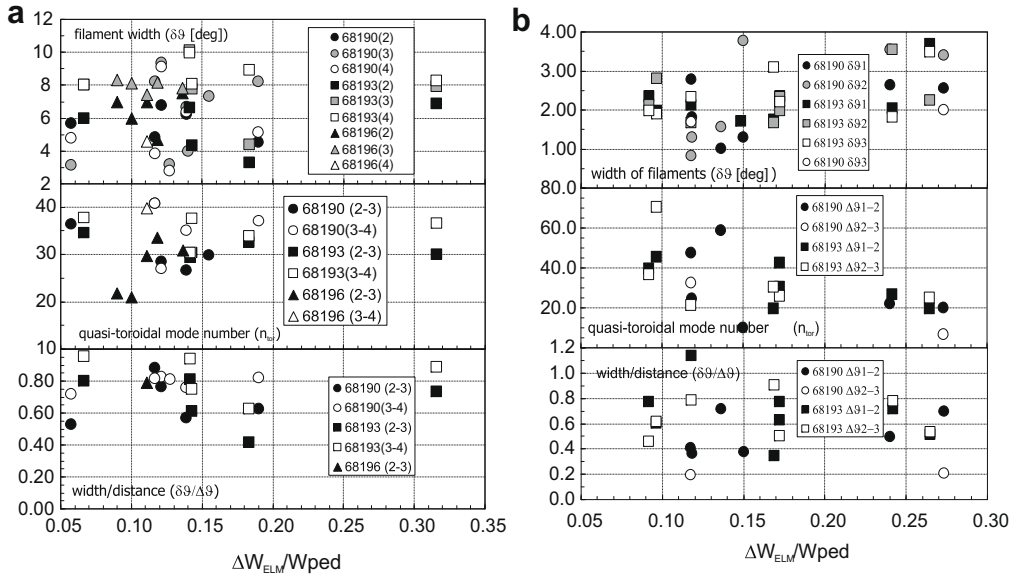

Fig. 4. Variation of filament footprints structure with ELM size for the outer limiters (a) and upper dump plates (b): top – footprint width ($\delta\vartheta$), middle – toroidal mode number $n_{\rm tor}$, bottom – ratio of the filament imprint width to the separation of the filaments ($\delta\vartheta/\Delta\vartheta$).

$\Delta W/W_{\rm ped} \approx 0.25$. Ratio of filaments width and separation cluster around value of $\delta\vartheta/\Delta\vartheta = 0.6 \pm 0.2$. Meanwhile, the toroidal mode number is monotonically decreasing with the ELM size from value of about 60 ($\Delta\vartheta \approx 3^\circ$) at $\Delta W/W_{\rm ped} \approx 0.1$ to value of $n_{\rm tor} \sim 20$ ($\Delta\vartheta \approx 5^\circ$) at $\Delta W/W_{\rm ped} \approx 0.28$. This is consistent with ELITE calculations shown by Snyder et al. in [17]. The calculations there are performed for three different densities showing that with the electron density increasing from 2×10^{19} m^{-3} to 6×10^{19} m^{-3} the range of most unstable modes shifts from (10–30) to (50–70). The size of ELMs is reduced as density is increased.

5. Summary

In this work we have performed extended analysis of the spatial structure of the filament footprints during Type-I ELMs on the plasma facing components on the outer limiters and upper dump plates of the JET main chamber. The data is obtained with help of a wide angle infrared diagnostic. The filaments are observed for Type-I ELMs in the energy range of $0.1\,MJ \leqslant \Delta W \leqslant 0.8\,MJ$ or $0.07 \leqslant \Delta W_{\rm ELM}/W_{\rm ped} \leqslant 0.32$ when normalized to the pedestal energy, which are typical ELM sizes in high power JET discharges. They have the form of narrow stripes when seen on the PFC and follow pre-ELM magnetic field lines and therefore they do not noticeably disturb/distort the SOL magnetic field. Typically one observes several filaments hitting the area of the first limited flux surface in the midplane region, especially in the area of shortest distance to the separatrix. The maximum observed temperatures on average highest for the central footprint of a set of more than one filaments. We have estimated quasi-toroidal mode number, which is the calculated inverse toroidal distance of two neighboring filaments, for the hot spots on the upper dump plates and outer limiters. Obtained value is about 12 for the low triangularity case, which is in rough agreement with the peeling-ballooning model and observation made at ASDEX Upgrade and MAST. In high triangularity the poloidal width of the filaments on the outer wall limiters is of order of 6° (10 cm). The poloidal distance between these filaments vary from 6 to 12° ($n_{tor} \sim 30$—40) on the outer wall limiters and from 2 to 6° ($n_{\rm tor} \sim 20$—60) on the dump plates confirming the high level of variability as reported from ASDEX Upgrade [10] and DIII-D [16]. In extension to ASDEX Upgrade results [10] the data presented here seems to show a monotonic change of filament footprints width and separation with the ELM size.

Acknowledgement

This work, supported by the European Communities under the contract of Association between EURATOM/IPP, was carried out within the framework of the European Fusion Development Agreement. The views and opinions expressed herein do not necessarily reflect those of the European Commission.

References

[1] F. Wagner et al., Plasma Phys. Control. Fusion 48 (2006) A217.
[2] Th. Eich et al., Phys. Rev. Lett. 43 (2003) 1145.
[3] A. Kirk et al., Phys. Rev. Lett. 96 (2004) 185001.
[4] M. Endler et al., Plasma Phys. Control. Fusion 47 (2005) 219.
[5] H.R. Wilson, S.C. Cowley, Phys. Rev. Lett. 92 (2004) 175006.
[6] Ph. Ghendrih et al., J. Nucl. Mater. 313–316 (2003) 914.
[7] P. Andrew et al., in: Contribution to 34th EPS Conference Plasma Physics, Warsaw, 2007.
[8] R.A. Pitts et al., Nucl. Fusion 47 (2007) 1437.
[9] A. Herrmann et al., Plasma Phys. Control. Fusion 46 (2004) 971.
[10] Th. Eich et al., Plasma Phys. Control. Fusion 47 (2005) 815.
[11] A. Herrmann et al., J. Nucl. Mater. 363–365 (2007) 528.
[12] W. Fundamenski et al., Plasma Phys. Control. Fusion 49 (2007) R43.
[13] Th. Eich et al., J. Nucl. Mater. 337–339 (2005) 669.
[14] R.A. Pitts et al., J. Nucl. Mater. 390–391 (2009) 755.
[15] J.A. Alonso et al., J. Nucl. Mater. 390–391 (2009) 797.
[16] J.H. Yu et al., in: Contribution to 34th EPS Conference on Plasma Physics, Warsaw, 2007..
[17] P. Snyder et al., Nucl. Fusion 44 (2004) 320328.